Characterization of pure and alloy metal superconductors

Vassilios Kaxiras* and Austin Li†
Department of Physics, Harvard University, Cambridge, Massachusetts 02138, USA
(Dated: April 8, 2025)

We present a theoretical overview of superconductivity, followed by an experimental investigation and classification of eleven metal samples as type I, type II, or non-superconducting. We observe the superconducting transition through measurements of the differential magnetization χ of each sample, and from the resistance of one sample. We estimate the transition fields and temperatures of one type I sample and one type II sample and determine the coherence length ξ and penetration depth λ of the former.

I. INTRODUCTION

Superconductivity was discovered in 1911 at Leiden University by H. Kamerlingh Onnes, who was the first to successfully liquefy helium and achieve cooling to a few degrees Kelvin [1]. What Onnes observed was that for certain metals, electrical resistance dropped sharply to zero below a certain critical temperature of a few Kelvin.

In this article, we aim to overview the basic properties of superconductors. We start by covering the prevailing theoretical understanding and discussing its key predictions. Subsequently, we investigate the superconducting transitions of eleven samples of seven different metals and one non-metal. We describe our setup, which consisted of a variable-temperature cryostat equipped to perform differential magnetization and resistance measurements.

We conclude by classifying our samples as non-superconducting, type I superconducting, or type II superconducting, and provide calculations of the transition fields and transition temperature for two samples, as well as estimates of the coherence length and penetration depth for one lead sample.

II. THEORY OF SUPERCONDUCTIVITY

The key properties of the superconducting state are:

1. Perfect conductivity (arbitrarily low electrical resistance), discovered by H. Kamerlingh Onnes [1].

2. The Meissner effect: expulsion of any magnetic field (Figure 1) from the interior of the sample beyond a penetration depth λ from the surface, discovered in 1933 by W. Meissner and R. Ochsenfeld [2].

All superconductors have a critical temperature T_c and a temperature-dependent critical magnetic field $H_c(T)$: at sufficiently high temperature and/or magnetic field, the superconducting state is destroyed and the material behaves regularly. Empirically, it has been observed that the critical field depends on temperature as

$$H_c(T) \approx H_c(0)\left[1-\left(\frac{T}{T_c}\right)^2\right]. \tag{1}$$

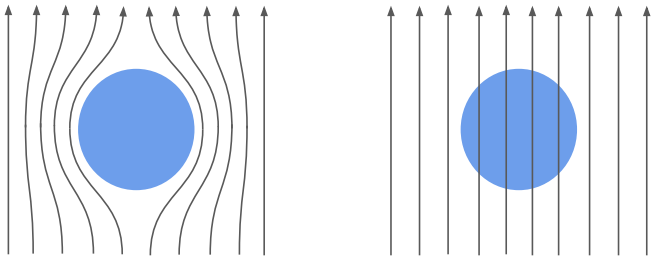

(a) Superconducting. (b) Regular.

FIG. 1: The Meissner effect: magnetic fields (depicted by field lines) are expelled in the superconducting state, but pass through unchanged in the regular state.

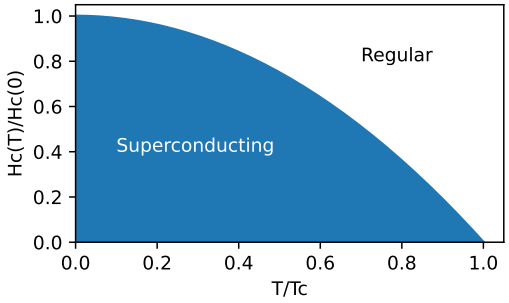

FIG. 2: Phase diagram of a simple superconductor, showing the superconducting state below the critical temperature T_c and the temperature-dependent critical field $H_c(T)$.

Similarly, the penetration depth has the following empirically observed temperature dependence:

$$\lambda(T) \approx \frac{\lambda(0)}{\sqrt{1-(T/T_c)^4}}. \tag{2}$$

* vkaxiras@college.harvard.edu
† awli@college.harvard.edu

This shows that λ diverges as $T \to T_c$ or $H \to H_c$ and the material becomes normal.

A. Phenomenological description

Phenomenologically, the perfect diamagnetism (Meissner effect) of superconductivity can be explained by presupposing perfect conductivity, through an analog of the Drude model with no dissipative factors.

We start by considering the effect of an electric field $\boldsymbol{E}$ on the current $\boldsymbol{J} = -ne\boldsymbol{v}$ of electrons with number density n in the absence of dissipation:

$$nm\frac{d\boldsymbol{v}}{dt} = -ne\boldsymbol{E} \implies \boldsymbol{E} = \Lambda\frac{d\boldsymbol{J}}{dt}, \quad \Lambda \equiv \frac{m}{ne^2}. \tag{3}$$

Now consider a magnetic field applied externally on such a superconducting sample. As the field is increased from zero, Faraday's Law will induce an electric field and loops of current. With Ampere's Law, this additional current will produce a magnetic field to cancel the applied field:

$$\begin{aligned} -\frac{d\boldsymbol{B}}{dt} = \nabla\times\boldsymbol{E} = \Lambda\frac{d}{dt}\nabla\times\boldsymbol{J} = \frac{\Lambda}{\mu_0}\frac{d}{dt}\nabla\times\nabla\times\boldsymbol{B} \\ = -\frac{\Lambda}{\mu_0}\frac{d}{dt}\nabla^2\boldsymbol{B} \implies \nabla^2\boldsymbol{B} = \frac{\mu_0}{\Lambda}\boldsymbol{B} \end{aligned} \tag{4}$$

where we used $\nabla\cdot\boldsymbol{B} = 0$ and neglected the typically minuscule displacement current. For a magnetic field of $\boldsymbol{B}_0$ at the boundary ($x = 0$) of an infinitely long superconductor, this has solutions

$$\boldsymbol{B}(x) = \boldsymbol{B}_0 e^{-x/\lambda}, \quad \lambda = \sqrt{\frac{\Lambda}{\mu_0}} \tag{5}$$

within the material.

Thus we see that the current loops screen out the magnetic field, up to a penetration depth λ. Note that the key difference from a regular conductor is that the lack of dissipative effects allow the current loops introduced from ramping up the field to remain even after the field is held constant, maintaining the screening effect for indefinite time.

The above relations, known as the London equations after Fritz and Heinz London [3], are summarized as

$$\boldsymbol{B} = -\Lambda\boldsymbol{\nabla}\times\boldsymbol{J}, \quad \boldsymbol{E} = \Lambda\frac{d\boldsymbol{J}}{dt}. \tag{6}$$

B. Bardeen–Cooper–Schrieffer theory

The first widely accepted microscopic theory of superconductivity was proposed by J. Bardeen, L. N. Cooper, and J. R. Schrieffer in 1957 [4], and is still widely accepted as the prevailing model for the microscopic properties of superconductors.

At the core of BCS theory is the presence of an attractive interaction $V(\boldsymbol{r}_1 - \boldsymbol{r}_2)$ between two electrons at positions $\boldsymbol{r}_1, \boldsymbol{r}_2$. Converting $\boldsymbol{r}_1, \boldsymbol{r}_2$ to the center of mass and relative coordinates $\boldsymbol{R} = (\boldsymbol{r}_1+\boldsymbol{r}_2)/2, \boldsymbol{r} = \boldsymbol{r}_1-\boldsymbol{r}_2$, and neglecting $\boldsymbol{R}$ due to translational invariance, the Fourier components of $V(\boldsymbol{r})$ can be identified:

$$V_{\boldsymbol{q}} \equiv \int V(\boldsymbol{r})e^{-i\boldsymbol{q}\cdot\boldsymbol{r}}d\boldsymbol{r} = \int e^{-i\boldsymbol{k}\cdot\boldsymbol{r}_1}e^{i\boldsymbol{k}\cdot\boldsymbol{r}_2}V(\boldsymbol{r})e^{i\boldsymbol{k}'\cdot\boldsymbol{r}_1}e^{-i\boldsymbol{k}'\cdot\boldsymbol{r}_2}d\boldsymbol{r} \tag{7}$$

where $\boldsymbol{k}$ is arbitrary and $\boldsymbol{k}' \equiv \boldsymbol{k}-\boldsymbol{q}$. This is evidently the scattering potential for a pair of electrons with equal and opposite momenta $(\boldsymbol{k}', -\boldsymbol{k}')$ into new momenta $(\boldsymbol{k}, -\boldsymbol{k})$. If this interaction has a negative sign, it can lead to bound superposition states of pairs of electrons with opposite momenta that are localized (relative to each each other):

$$\sum_{\boldsymbol{k}} g_{\boldsymbol{k}}e^{i\boldsymbol{k}\cdot\boldsymbol{r}_1}e^{-i\boldsymbol{k}\cdot\boldsymbol{r}_2} = \sum_{\boldsymbol{k}} g_{\boldsymbol{k}}e^{i\boldsymbol{k}\cdot\boldsymbol{r}}. \tag{8}$$

This as well as the rest of the features of superconductivity can be observed within the so-called BCS pairing Hamiltonian, which adds the aforementioned pair scattering term to the standard electron gas energy spectrum. The pairing Hamiltonian is:

$$H = \sum_{\boldsymbol{k},\sigma}\epsilon_{\boldsymbol{k}}n_{\boldsymbol{k}\sigma} + \sum_{\boldsymbol{k},\boldsymbol{l}}V_{\boldsymbol{k}\boldsymbol{l}}a^\dagger_{\boldsymbol{k}\uparrow}a^\dagger_{-\boldsymbol{k}\downarrow}a_{-\boldsymbol{l}\downarrow}a_{\boldsymbol{l}\uparrow} \tag{9}$$

where $a^\dagger_{\boldsymbol{k}\sigma}, a_{\boldsymbol{k}\sigma}$ are the fermionic creation and annihilation operators for electrons with momenta $\boldsymbol{k}$ and spin σ, $n_{\boldsymbol{k}\sigma} = a^\dagger_{\boldsymbol{k}\sigma}a_{\boldsymbol{k}\sigma}$ is the number operator, and $\epsilon_{\boldsymbol{k}} = \frac{\hbar^2k^2}{2m_e}$ are the plane-wave energies, which when unperturbed produce a continuous spectrum in the bulk limit:

$$\epsilon_{\boldsymbol{k}+\boldsymbol{dk}} - \epsilon_{\boldsymbol{k}} \le \frac{\hbar^2}{2m}((k+dk)^2 - k^2) = \frac{\hbar^2k}{m}dk. \tag{10}$$

The key property of the BCS Hamiltonian from which superconductivity arises is a non-trivial spectral gap Δ (energy difference between the first two states), in contrast to the continuous spectrum above. If the interaction terms $V_{\boldsymbol{q}}$ are non-positive, a gapped ground state of lower energy than the standard Fermi sea at $T = 0$ appears.

Because the attractive interaction between electrons leads to bound states of pairs of electrons with opposite momenta, BCS posits that the superconducting ground state consists of many such states, called Cooper pairs, all together giving a total momentum of 0. The ground state energy gap Δ then gives the energy needed to break a single Cooper pair at the Fermi surface, as that is the smallest excitation possible from this ground state.

The fact that the ground state is gapped also means that at sufficiently low temperatures ($\ll \Delta/k_B$), the system momentum will largely remain at 0. Introducing the canonical momentum $\boldsymbol{p} = m\boldsymbol{v} - e\boldsymbol{A}$ of an electron in a magnetic vector potential $\boldsymbol{A}$, we see that if the momentum is fixed at 0, then the velocity must change when we introduce $\boldsymbol{A}$, giving

$$\boldsymbol{v} = \frac{e\boldsymbol{A}}{m}. \tag{11}$$

The corresponding supercurrent with electron carrier density n reproduces the London equations discussed above:

$$\boldsymbol{J} = -ne\boldsymbol{v} = -\frac{ne^2}{m}\boldsymbol{A} \implies \boldsymbol{B} = \nabla \times \boldsymbol{A} = -\Lambda \nabla \times \boldsymbol{J}, \tag{12}$$

justifying the Meissner effect.

As temperature T increases, in a mean-field treatment the thermodynamic energy gap $\Delta(T)$ — defined as the energy needed to break a Cooper pair at the Fermi surface in the presence of a thermal sea of broken and unbroken pairs — decreases as more pairs are broken. Clearly, $\Delta(0) = \Delta$; as T increases, Δ approaches zero at the critical temperature T_c, where superconductivity is destroyed. BCS theory predicts the following relationships for superconductors with weak electron-electron interactions:

$$\Delta(0) = 1.764 k_B T_c, \quad \frac{\Delta(T)}{\Delta(0)} \approx 1.74\sqrt{1 - \frac{T}{T_c}},\ T \approx T_c. \tag{13}$$

The ground state gap Δ also leads to an expression for the condensation energy at zero temperature of a sample with N electrons:

$$U_n(0) - U_s(0) = \frac{1}{2}N(0)\Delta^2(0). \tag{14}$$

Identifying this with the energy required to screen out a field $\mu_0 H^2/2$ (see Eq. 22), we obtain a relationship for the zero-temperature critical field H_c beyond which the energy required for the Meissner effect exceeds the condensation energy of the superconducting state, and the material becomes normal:

$$H_c(0) = \Delta(0)\sqrt{N(0)/\mu_0}. \tag{15}$$

Lastly, perfect conductivity is explained in the BCS theory simply from the presence of the energy gap, which forces any dissipative process to excite the entire many-body wave function by the non-trivial gap value.

C. Ginzburg-Landau theory

A powerful macroscopic theory of superconductivity in the context of thermodynamic phase transitions was introduced by Vitaly Ginzburg and Lev Landau in 1950 [2]. The Ginzburg-Landau (GL) theory defines a pseudowavefuncion ψ that represents the density of superconducting charge carriers n^*, such that $n^* = |\psi|^2$. It then postulates an expansion of the free energy F_s:

$$F_s = F_{n0} + \frac{\mu_0 H^2}{2} + \alpha n^* + \frac{\beta}{2}(n^*)^2 + \frac{1}{2m^*}|(-i\hbar\nabla - e^*\boldsymbol{A})\psi|^2 \tag{16}$$

where F_{n0} is the free energy density of the regular state at zero field, $\mu_0 H^2/2$ is the energy required to diamagnetically screen out a field H (see Eq. 22), and the next two terms represent a general second-order expansion of the free energy dependence on the density of superconducting electrons. The last term can be rewritten as

$$n^*\frac{1}{2}m^* v_s^2 + \frac{\hbar^2}{2m^*}(\nabla|\psi|)^2 \tag{17}$$

where the first component represents the kinetic energy contribution of the supercurrent of velocity v_s, and the second adds dependence on the curvature of ψ and is associated with surface energy between domains. The charge carriers in this model have mass m^* and charge e^*; assuming Cooper pair charge carriers, these can be taken to be twice the values for the electron.

The thermodynamic equilibrium state of a superconductor is determined by minimizing the free energy F_s, expressed by the GL differential equation $dF/d\psi = 0$. This involves a trade-off between all the components mentioned above.

In the context of this thermodynamic treatment, several parameters arise. We list them here and reference the reader to Chapter 4 of M. Tinkham's "Introduction to Superconductivity" [2] for further discussion:

1. The penetration depth λ_{eff}, which takes the same form as in the London equations:

$$\lambda_{\text{eff}} \equiv \sqrt{\frac{m^*}{n^*(e^*)^2\mu_0}}. \tag{18}$$

2. The characteristic length scale of the wave function ξ, associated with the value of its second derivative:

$$\xi \equiv \sqrt{\frac{\hbar^2}{2m^*|\alpha|}}. \tag{19}$$

We can briefly see the origin of this expression by considering the free energy minimization condition $dF_s/d\psi = 0$, taking $\boldsymbol{A} = H = \beta = 0$ and ψ to be real for simplicity:

$$\frac{1}{2}\frac{dF_s}{d\psi} = \alpha\psi + \frac{\hbar^2}{2m^*}\nabla^2\psi = 0 \implies \nabla^2\psi = -\frac{1}{\xi^2}\psi \tag{20}$$

which has solutions in 1 dimension of the form $e^{ix/\xi}$.

Notably, at length scales much smaller than ξ, we expect the wave-function not to vary significantly.

3. The Ginzburg-Landau dimensionless parameter κ:

$$\kappa \equiv \frac{\lambda_{\text{eff}}(T)}{\xi(T)} = \sqrt{2}e^* H_c(T)\lambda_{\text{eff}}^2(T)/\hbar. \tag{21}$$

The relation with $H_c, \lambda_{\text{eff}}$ is determined from minimizing the GL free energy expression (Eq. 16) and substituting the definition of H_c (Eq (22). While some temperature dependence is perhaps expected from the equation above, κ typically varies very slowly with T.

4. The thermodynamic critical field H_c. This is defined as the field at which the energy required to screen out the magnetic field exceeds the free energy difference between the normal and superconducting state (at zero field). In the perfect diamagnetic case (the Meissner effect) with magnetization $\boldsymbol{M} = -\boldsymbol{H}$

$$F_{n0} - F_{s0} = -\int_0^{H_c} \boldsymbol{M} \cdot (\mu_0 d\boldsymbol{H}) = \frac{\mu_0 H_c^2}{2}. \tag{22}$$

5. The bulk nucleation field H_{c_2}, below which superconducting regions can form within the material. Beyond this value, there are no non-zero solutions for ψ to the GL equation $dF/d\psi = 0$. This is given by

$$H_{c_2} = \kappa\sqrt{2} H_c. \tag{23}$$

6. The penetration field H_{c_1}. Above this field, it is thermodynamically favorable for flux to penetrate the material. For $\kappa \gg 1$, this is given by

$$H_{c_1} \approx \frac{\ln \kappa}{\kappa\sqrt{2}} H_c. \tag{24}$$

Ginzburg and Landau, and later Alexei Abrikosov and Lev Gor'kov [2], distinguished between two types of superconductors with radically different properties, emergent from the GL theory. These properties are summarized in Table I:

TABLE I: Key differences between type I and type II superconductors. γ is the surface energy, defined as the free energy per unit area of boundaries between superconducting and normal regions. PT is short for phase transition.

Type I	Type II
$\kappa < 1/\sqrt{2}$	$\kappa > 1/\sqrt{2}$
$\gamma > 0$	$\gamma < 0$
$H_{c_2} < H_c$	$H_{c_2} > H_c$
1st order PT	2nd order PT
Supercooling	No supercooling

Type I superconductors have positive surface energy γ, so it is favorable to minimize the number of boundaries and thus the type I state is typically either entirely superconducting (with very little flux penetration) or entirely normal. On the other hand, type II materials have negative γ, so there is penetrating flux in an intermediate state above H_{c_1} where the material subdivides into normal regions and superconducting "vortices" (analogous to microscopic supercurrent loops) on the scale of ξ, maximizing the total boundary area.

Type I and type II superconductors are further distinguished by the relationship between H_c and H_{c_2}. Since a type I samples has $H_{c_2} < H_c$, when approaching the superconducting transition from high field it can "supercool", remaining in the superconducting state below H_c until H_{c_2} is reached and superconducting regions can nucleate in a rapid, first-order transition. When approaching the transition from low field, the sample remains superconducting past H_{c_2} until a first order phase transition at H_c. In contrast, a type II superconductor has $H_{c_1} < H_c < H_{c_2}$, so it will have a smooth second-order transition in both directions between H_{c_1} to H_{c_2}.

III. EXPERIMENTAL SETUP

A. Cryostat

We used a Janis model 8DT variable-temperature cryostat (pictured in Figure 3) with two cryogenic reservoirs: one (the outer chamber) for liquid nitrogen and the other (the inner chamber) for liquid helium. At the center of the cryostat was the sample chamber, which was suspended below the main reservoirs and within a large electromagnet, and isolated from the surrounding reservoirs via a vacuum jacket. After transferring nitrogen and helium to the reservoirs, cooling of the sample was initiated by opening the helium needle valve and transferring a small amount of liquid into the bottom of the sample chamber. This helium was then vaporized by the heater, and maintained at a constant temperature via a feedback loop through a temperature sensor (sensor "A") at the bottom of the chamber. The temperature sensor was a model TG-120P GaAlAs diode, controlled by a Lake Shore Cryotronics model 805 temperature controller. This allowed temperature control above 4.2 K. For control below 4.2 K, a larger amount of liquid helium (1-2 liters) were transferred to the sample chamber, which was then closed off from the helium reservoir. With the heater turned off the sample chamber was then vacuum pumped and the temperature was determined from the vapor pressure of helium.

B. Sample chamber

The sample chamber contained our ten metal and nonmetal samples. The samples were labelled Cu (copper); In (indium); In2Bi (a 98-2 indium-bismuth alloy); In4Bi (a 96-4 indium-bismuth alloy); Pb0, Pb1, and Pb2 (lead); PTFE (Teflon); Sn (tin); and SnPb (a a 60-40 tin-lead alloy). Each sample was cylindrical with its long axis oriented along the magnetic field direction, 16 mm long and 1 mm in diameter, with 240 turns of #40 varnished magnet wire wrapped in 2 layers around them, except for samples Pb0 and Pb1. Pb1 had a single layer of 120 turns of wire, while Pb0 was 6 mm long and 3/4 mm in diameter with a single layer of 40 turns. The magnetic wire was used for inductive measurements of the differential magnetization (see Eq. 26). The samples were placed in

a sample holder within the sample chamber. The combined configuration and one example sample are shown in Figure 4.

There was an eleventh sample in the chamber in a different configuration. This sample was the same material as the SnPb sample, but arranged in a thin ribbon roughly 1 m x 2 mm x 0.1 mm in size when wound, and on the order of 1 meter when unwound. This sample was wound non-inductively and four contacts (2 for current, 2 for voltage) were placed at its ends to perform a four-probe resistance measurement.

Temperature at the samples themselves (slightly above the bottom of the chamber) was measured by a second TG-120P GaAlAs diode (sensor "B") connected to the same Lake Shore Cryotronics temperature controller mentioned in the cryostat description.

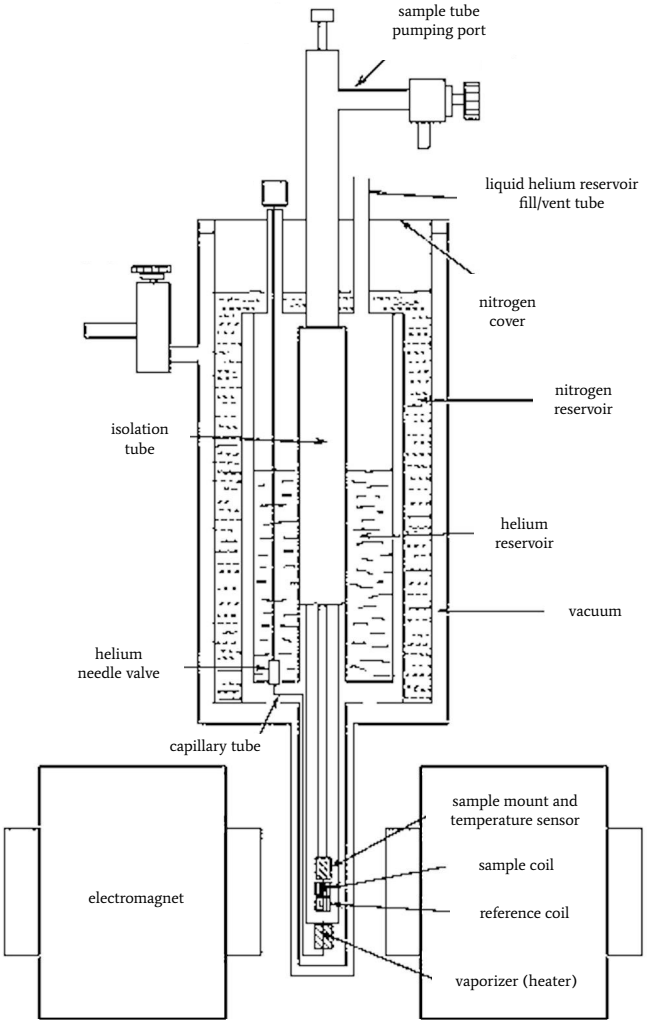

FIG. 3: Our cryostat setup.

C. Magnetic field control and measurement

An 12-inch diameter poleface Varian electromagnet surrounding the sample chamber applied a field along the cylindrical axes of the samples. The magnet was controlled by a Kepco BOP 20-20M amplifier capable of driving a DC magnetic field up to 2.4 kGauss, although we did not exceed 1 kGauss in our experiment. The field was measured less than 1 cm from the outside of the sample chamber with a Bell HTB1-0608 transverse Hall probe controlled by a Bell 615 Gaussmeter. We calibrated the Gaussmeter's analog output with its magnetic field readings.

D. LF setup

For differential magnetization measurements, the magnetic field was AC modulated by two coils placed on the inner sides of the electromagnet. These coils were driven by a function generator and amplifier (Kepco BOP 20-5M) at a range of frequencies, from 23 Hz to 53 Hz in increments of 10 Hz, and an amplitude of 1.75 Vpp. This induced an AC magnetization within the samples, whose amplitude was measured by extracting the induced voltage at the modulation frequency with a lock-in amplifier. For these measurements, the lock-in amplifier was set to 200 μV sensitivity and an integration time constant of 30 ms.

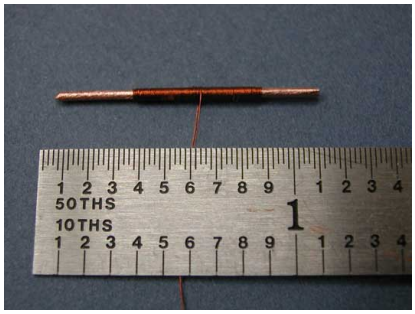

(a) The copper sample (Cu).

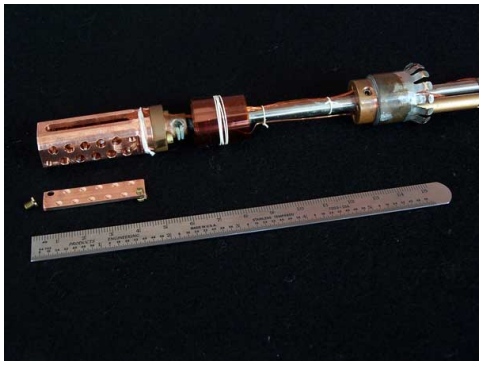

(b) The sample holder.

FIG. 4: The sample chamber.

For resistivity measurements, the function generator and Kepco amplifier drove the 2 current probes of the sample at a range of frequencies from 33 Hz to 237 Hz and an amplitude of 2.5 Vpp, while the 2 voltage probes were connected to the lock-in amplifier to extract the voltage across the sample. The lock-in amplifier was set to a sensitivity of 200 μV and a time constant of 3 s. The resistivity of the current probes at 110 Kelvin was measured to be 0.756 Ohms, and the driving current at the current probes was calculated to be 17.3 μA_{rms}.

E. Data collection

The analog outputs of the lock-in amplifier and Gaus smeter were fed into a National Instruments PCIe-6321 interface card, controlled by a Windows desktop running our analysis software written in National Instruments LabView.

IV. METHODOLOGY

A. Meissner effect measurements

In the superconducting state, the Meissner effect implies the samples become perfectly diamagnetic to cancel the field H, that is:

$$0 = B = \mu_0(H + M) \implies \frac{M}{H} = -1. \tag{25}$$

Detecting this by measuring M directly was impossible, however, as we could not detect the magnetic field inside a sample without having a probe inside it. Instead, we used Faraday's Law to measure the magnetization within a time-varying field $H(t) = H_0 e^{i\omega t}$ applied by the modulation coils, which induced a voltage in the coils wrapped around the samples:

$$\mathcal{E} \propto \frac{dB}{dt} \propto \frac{dH}{dt} + \frac{dM}{dt} = \frac{dH}{dt}(1 + \chi), \quad \chi \equiv \frac{dM}{dH} \tag{26}$$

where χ is known as the differential magnetization. Thus

$$\frac{dH}{dt} = i\omega H_0 e^{i\omega t} \implies \mathcal{E} \propto e^{i\omega t}(1 + \chi). \tag{27}$$

Assuming we could cancel the unity term, this implied measuring the $e^{i\omega}$ component of $\mathcal{E}$ gives the differential magnetization χ. Cancellation of the unity term was done to some degree by a counter-wound section of the inductance wire, but it was not perfect. Therefore we expected the relationship between the signal from the lock-in amplifier ε and χ to be an arbitrary linear one:

$$\varepsilon = a\chi + b, \quad a, b \in \mathbb{C}. \tag{28}$$

As discussed, in the superconducting state χ should have been a negative constant. In the regular state, it should have been around 0 since all of our samples were very weakly magnetic. Following the GL theory, above H_c and H_{c_2}, we expected $\chi \approx 0$ and below H_{c1} and H_c, we expected $\chi < 0$. A sharp transition in χ should have occurred at H_c for type I when sweeping from low to high field and at $H_{c_2} < H_c$ when sweeping from high to low. A slow transition should have occurred over $H_{c_1} < H < H_{c_2}$ for type II, perhaps with a feature at H_{c_1} corresponding to the introduction/expulsion of flux.

For each sample, we obtained $\chi(H)$ measurements by sweeping H with a triangular ramp of period 100 seconds and amplitude 1 kGauss.

B. Peak finding

In order to classify the samples, we employed different algorithms and techniques to extract critical fields and temperatures from our raw $\chi(H)$ data. Because we swept the field in both directions, we first isolated a range of field values to observe. The field values we chose to isolate correspond to our magnetic field sweeping from the minimum to maximum value.

After we isolated this range, we performed peak-finding to find the transition fields H_c, H_{c_2} for type I superconductors and H_{c_1}, H_{c_2} for type II superconductors. For type I superconductors, we used:

$$H_{c_2} = \max_H \{\chi(H) : H \le 0\}, \qquad H_c = \max_H \{\chi(H) : H > 0\}. \tag{29}$$

We expected $H_c > H_{c_2}$ in accordance with GL theory.

For type II superconductors, finding the transition fields was not so simple. H_{c_1} occurred in the trough of the $\chi(H)$ graph and there were no well-defined points to extract H_{c_2}. Moreover, the noise in the system increased the difficulty of finding a peak. Because of these difficulties, we decided to employ curve-fitting techniques.

To eliminate noise and smoothen out our data, we fit our $\chi(H)$ data to a function of the form

$$f(x) = A\left[\frac{1}{1 + e^{k(x+x_0)}} + \frac{1}{1 + e^{-k(x-x_0)}}\right] + f(0) \tag{30}$$

to extract optimal parameters $\{A, k, x_0, f(0)\}$.

We then calculated the absolute derivative $|df/dx|$ and extracted the fields corresponding to the two maximal values of $|df/dx|$. Let H_{p_1}, H_{p_2} denote these field values. These peak values defined the ranges of values we searched to determine H_{c_1}, H_{c_2}.

To find H_{c_1}, we searched the inner range of the derivative $[H_{p_1}, H_{p_2}]$, with boundaries defined by some *internal tolerance* t_{int} to extract x_{c_1}; to find H_{c_2} values, we searched the tails $(-\infty, H_{p_1}) \cup (H_{p_2}, \infty)$, with boundaries defined by some *external tolerance* t_{ext} to extract x_{c_2}.

We took

$$x_{c_1} = \min_x \left\{ \left| \frac{df(x)}{dx} \right| - t_{\text{int}} = 0 : x \in [H_{p_1}, H_{p_2}] \right\} \tag{31}$$

$$x_{c_2} = \min_x \left\{ \left| \frac{df(x)}{dx} \right| - t_{\text{out}} = 0 : x \in (-\infty, H_{p_1}) \cup (H_{p_2}, \infty) \right\} \tag{32}$$

with

$$H_{c_1} = \min_H \{|\chi(H) - f(x_{c_1})|\}, \quad H_{c_2} = \min_H \{|\chi(H) - f(x_{c_2})|\} \tag{33}$$

In other words, we found values x_{c_1}, x_{c_2} where the derivative was closest to our tolerances $t_{\text{int}}, t_{\text{out}}$ and found H_{c_1}, H_{c_2} by finding values where our data $\chi(H)$ was closest to the value at our fitted function $f(x_{c_i})$.

C. Resistivity measurements

In the superconducting phase, we expected electrical resistance to drop to near zero. As a result, we had to be careful about measuring it: any stray resistances from the probes or wires of the setup could potentially dominate the resistance of the sample. A four probe measurement solved this problem by driving all the current for the measurement through two current probes, and measuring the voltage across the sample with two voltage probes and a minuscule amount of current (on the order of 10μA) through them. Given the current I at the current probes and the voltage measurement V, the resistance of the sample was calculated as $R = V/I$. As discussed in the experimental setup, we estimated $I = 17.3\,\mu\text{A}_{\text{rms}}$.

V. RESULTS

A. Critical fields and temperatures

We generated $\chi(H)$ plots for all the samples, shown in Figure 9.

Using multiple χ measurements at different temperatures we were able to determine $H_c(T)$ for two samples, Pb2 and In4Bi. $H_c(T)$ for lead (Pb2) is shown in Figure 5, and $H_c(T)$ for the 96/4 indium-bismuth alloy is shown in Figure 6.

B. Sample classification

From Figure 9, we present the following classifications from our experiment by distinguishing the rapid first order transition of type I from the slow second order transition of type II in Table II.

We note that for type I superconductors we observe that $H_{c_2} < H_c$ for all of our samples, and for type II superconductors, we observe that $H_{c_1} < H_{c_2}$, in alignment with GL theory.

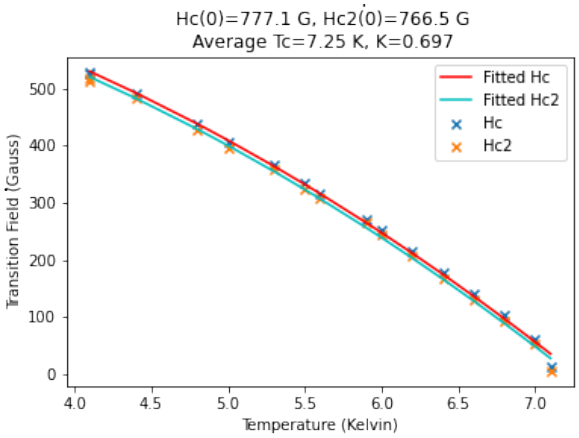

FIG. 5: Critical magnetic field of lead (Pb2).

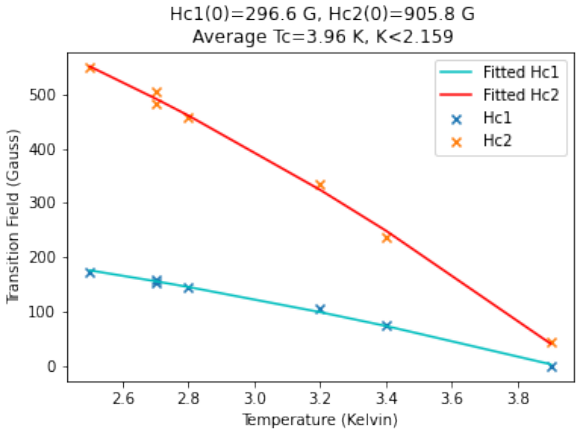

FIG. 6: Critical magnetic field of 96/4 indium-bismuth alloy.

TABLE II: Characterization of samples.

type I	type II	Non-superconducting
Indium	98/2 indium-bismuth	Copper
Lead (Pb0)	96/4 indium-bismuth	Teflon (PTFE)
Lead (Pb1)		
Lead (Pb2)		
Tin		
60/40 tin-lead		

C. Parameter estimation

We curve-fitted our $H_c(T)$ plots for lead (Pb2) and the 96/4 indium-bismuth alloy (In4Bi) to Eq. 1, allowing us to extrapolate estimates of $H_c(0), H_{c_1}(0), H_{c_2}(0)$ and to calculate κ using the theoretical relations above.

We note that κ for lead could be estimated using Eq. 23, and for In4Bi could be estimated with Eq. 24 if $\kappa \gg 1$. We were thus able to obtain a value of

$$\kappa_{\text{Pb2}} = 0.697 < \frac{1}{\sqrt{2}} \tag{34}$$

as expected.

We found no real solutions to the transcendental equation Eq. 24 for In4Bi, implying κ is near 1. Assuming $H_{c_1} < H_c$, we derived an upper bound using Eq. 23.

$$\frac{1}{\sqrt{2}} < \kappa_{\text{In4Bi}} < 2.159. \tag{35}$$

Additionally, for Pb2 we calculated $\lambda(0), \xi(0)$ using $H_c(0)$ and Eq. 21, obtaining the following values:

$$\boxed{\lambda_{\text{Pb2}}(0) = 457 \text{ Å}, \qquad \xi_{\text{Pb2}}(0) = 655 \text{ Å}.} \tag{36}$$

D. Resistance

We first note that the resistance sample was a type I superconductor. Because the sample was type I, we expected a very sharp change in resistance as the material transitioned from superconducting to non-superconducting. Thus we opted to take the midpoint between the minimum and maximum resistance:

$$T_c = T\left(\frac{1}{2}(\max R - \min R)\right). \tag{37}$$

We did this for many different frequencies and plotted them in Figure 7.

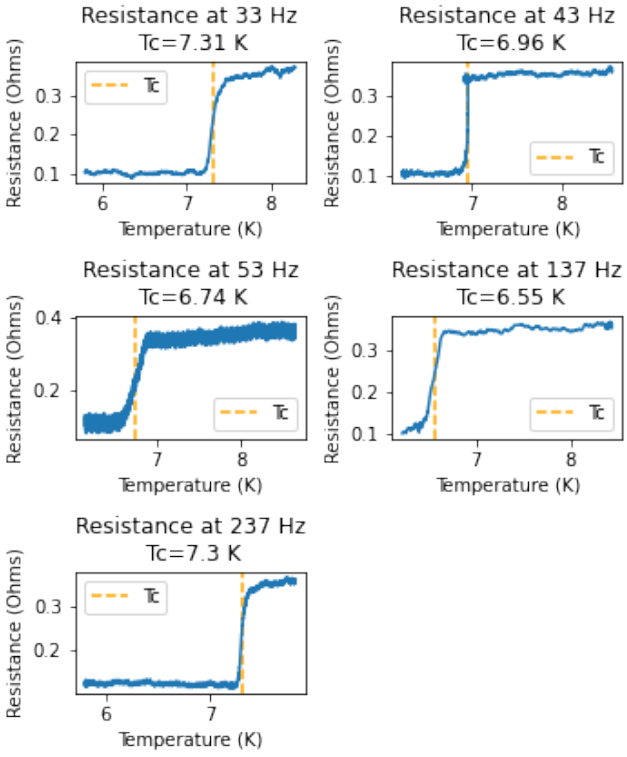

FIG. 7: Resistance of 60/40 tin-lead alloy sample.

We then plotted min $R(T)$ in Figure 8. We observe that the data is not what we expected. We should have seen the resistance increase with frequency, allowing us to extrapolate to zero frequency to obtain the DC resistance. This discrepancy is due to poor data collection. The raw data was collected as $R(t)$; in order to generate temperature plots, we needed to fit a function $T(t)$ where T is temperature and t time. We did this by manually recording the temperature in ten second intervals for about two minutes in order to determine how temperature varied by time. Because this data collection was manual and sparse, there was likely a large amount of experimental error.

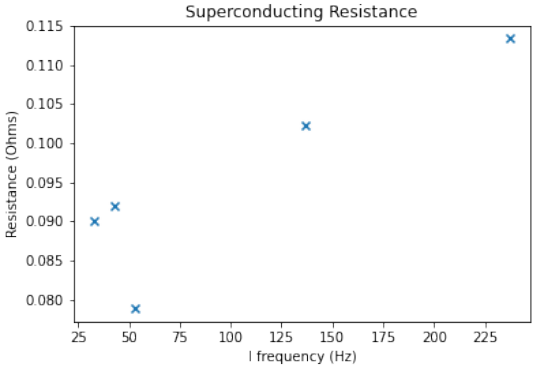

FIG. 8: Superconducting resistance of 60/40 tin-lead alloy sample.

VI. ACKNOWLEDGEMENTS

We would like to thank Professor Isaac Silvera and Professor Amir Yacoby for their theoretical and experimental guidance on the project and Joseph Peidle, Jieping Fang for their assistance in the lab.

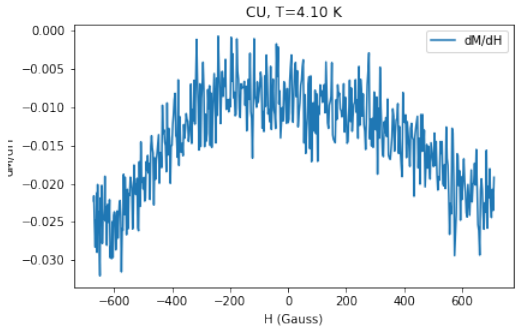

(a) Differential magnetization of copper.

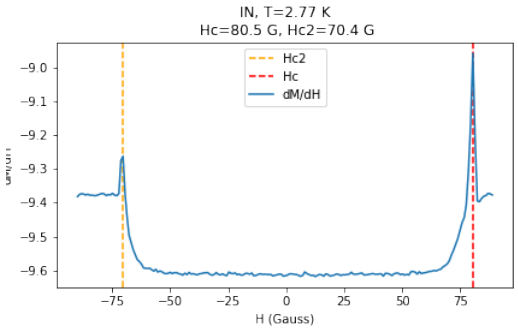

(b) Differential magnetization of indium.

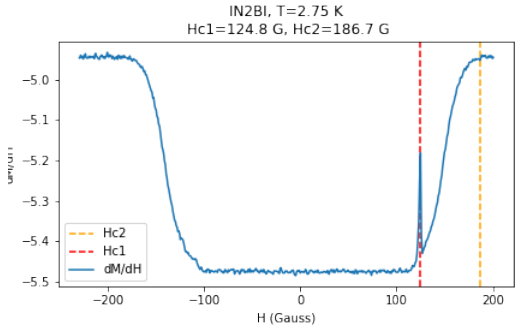

(c) Differential magnetization of 98/2 indium-bismuth alloy.

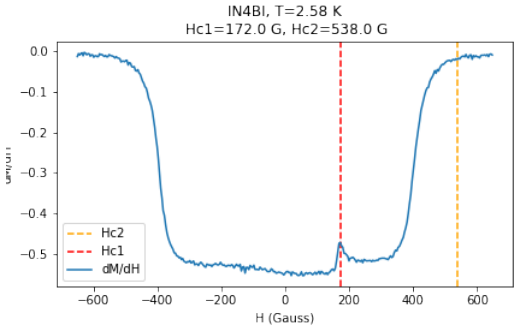

(d) Differential magnetization of 96/4 indium-bismuth alloy.

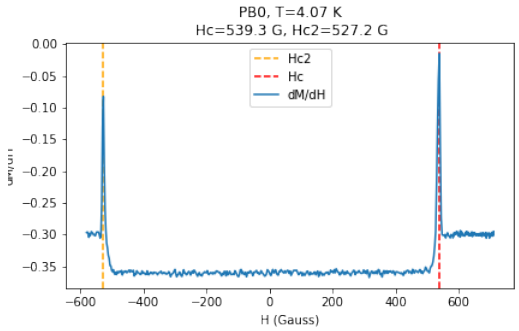

(e) Differential magnetization of lead (Pb0).

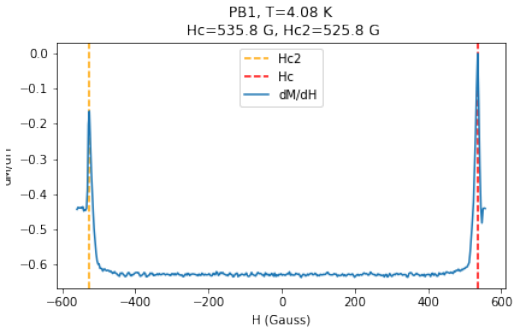

(f) Differential magnetization of lead (Pb1).

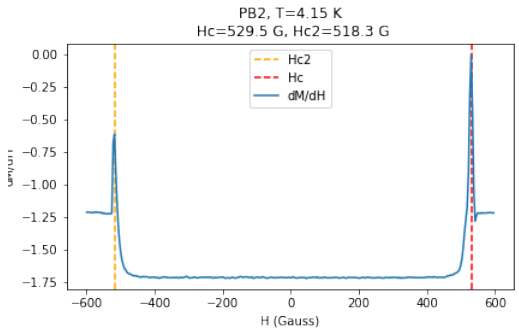

(g) Differential magnetization of lead (Pb2).

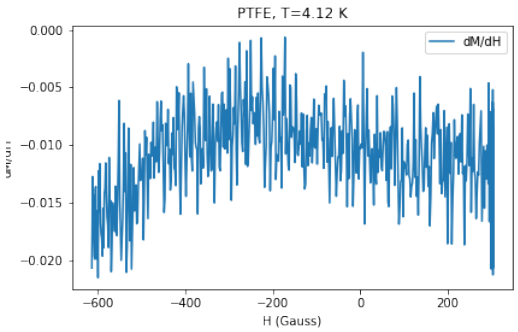

(h) Differential magnetization of Teflon (PTFE).

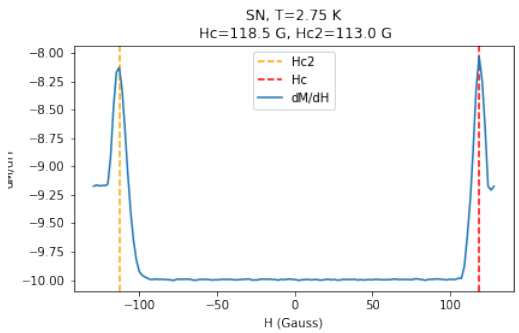

(i) Differential magnetization of tin.

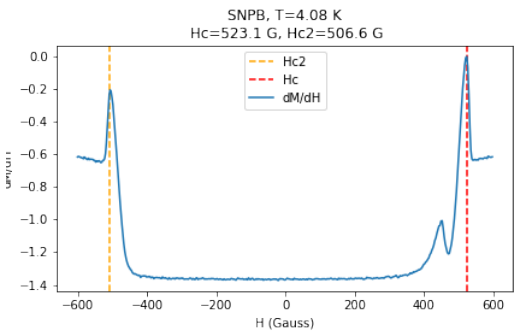

(j) Differential magnetization of 60/40 tin-lead alloy.

FIG. 9: $\chi(H)$ at selected temperatures for all 10 Meissner effect samples.

[1] K. Gavroglu, H. Onnes, and Y. Goudaroulis, *Through Measurement to Knowledge: The Selected Papers of Heike Kamerlingh Onnes 1853–1926*, Boston Studies in the Philosophy and History of Science (Springer Netherlands, 2012).

[2] M. Tinkham, *Introduction to Superconductivity*, Dover Books on Physics Series (Dover Publications, 2004).

[3] The electromagnetic equations of the supraconductor, Proceedings of the Royal Society of London. Series A - Mathematical and Physical Sciences **149**, 71 (1935).

[4] J. Bardeen, L. N. Cooper, and J. R. Schrieffer, Theory of superconductivity, Phys. Rev. **108**, 1175 (1957).